Biochemistry

pubs.acs.org/biochemistry Article

A Single-Point Mutation in D-Arginine Dehydrogenase Unlocks a Transient Conformational State Resulting in Altered Cofactor Reactivity

Archana Iyer, Renata A. G. Reis, Swathi Gannavaram, Mohamed Momin, Alexander M. Spring-Connell, Yoelvis Orozco-Gonzalez, Johnson Agniswamy, Donald Hamelberg, Irene T. Weber, Samer Gozem, Siming Wang, Markus W. Germann, and Giovanni Gadda*

Cite This: *Biochemistry* 2021, 60, 711–724 Read Online

ACCESS | Metrics & More | Article Recommendations

ABSTRACT: Proteins are inherently dynamic, and proper enzyme function relies on conformational flexibility. In this study, we demonstrated how an active site residue changes an enzyme's reactivity by modulating fluctuations between conformational states. Replacement of tyrosine 249 (Y249) with phenylalanine in the active site of the flavin-dependent D-arginine dehydrogenase yielded an enzyme with both an active yellow FAD (Y249F-y) and an inactive chemically modified green FAD, identified as 6-OH-FAD (Y249F-g) through various spectroscopic techniques. Structural investigation of Y249F-g and Y249F-y variants by comparison to the wild-type enzyme showed no differences in the overall protein structure and fold. A closer observation of the active site of the Y249F-y enzyme revealed an alternative conformation for some active site residues and the flavin cofactor. Molecular dynamics simulations probed the alternate conformations observed in the Y249F-y enzyme structure and showed that the enzyme variant with FAD samples a metastable conformational state, not available to the wild-type enzyme. Hybrid quantum/molecular mechanical calculations identified differences in flavin electronics between the wild type and the alternate conformation of the Y249F-y enzyme. The computational studies further indicated that the alternate conformation in the Y249F-y enzyme is responsible for the higher spin density at the C6 atom of flavin, which is consistent with the formation of 6-OH-FAD in the variant enzyme. The observations in this study are consistent with an alternate conformational space that results in fine-tuning the microenvironment around a versatile cofactor playing a critical role in enzyme function.

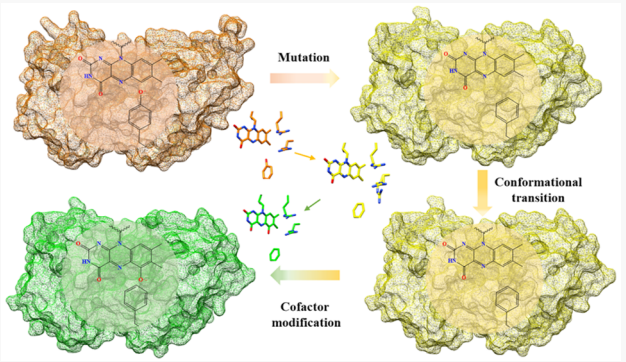

Enzymes catalyze chemical reactions in biological processes.[1] Understanding how enzymes perform otherwise inaccessible reactions under physiological conditions has been of interest for both fundamental and applied purposes. A majority of biochemical and structural studies have focused on the electrostatic contribution to enzyme catalysis.[2] While the inherent flexibility observed in enzymes is widely accepted to play a role in substrate capture and product release, the contribution of dynamic processes to enzyme catalysis is still not entirely accepted and well understood.[3,4] All proteins are inherently dynamic and exist in solution as ensembles of conformations.[5−7] Protein motions span a wide range of time scales, from ultrafast atom vibrations occurring on subpicosecond time scales and fast side-chain motions occurring on subnanosecond time scales to slow domain movements ranging from microseconds to seconds.[5,8,9] Conformational changes in enzymes facilitate many events like substrate capture, stabilization of transition states, and product release, which are essential for enzyme function.[10] The role of dynamics in catalysis has been investigated in many enzymes.[11,12] Different stages of catalysis, such as the binding of substrate and *cis*/*trans* isomerization, often require conformational changes in enzymes.[5,13,14]

Protein conformations can be pooled into conformational "substates" based on structural and energetic similarities.[15−17] Methods like nuclear magnetic resonance (NMR) relaxation dispersion have previously demonstrated the existence of such transient and sparsely populated conformational substates.[6,11,18,19] Early studies of myoglobin by Frauenfelder et al. in 1982 revealed multiple conformational substates that are

Received: January 19, 2021
Revised: February 16, 2021
Published: February 25, 2021

https://dx.doi.org/10.1021/acs.biochem.1c00054
Biochemistry 2021, 60, 711–724

coupled to function.[12,13,17,20−22] The population and sampling of protein conformational substates can be modulated by site-specific mutations, as demonstrated in bacterial phosphotriesterase, *Escherichia coli* dihydrofolate reductase (*Ec*DHFR), and cyclophilin A/proline isomerase.[11,23−25] Studies of *Ec*DHFR variants established that while the wild-type and mutant enzymes are similar in structure, they vary significantly in their ability to access specific conformational substates.[11]

D-Arginine dehydrogenase (EC 1.4.99.6, UniProtKB Q9HXE3, *Pa*DADH) from *Pseudomonas aeruginosa* PAO1 is an FAD-dependent enzyme that oxidizes D-arginine to 2-imino-arginine.[26] The enzyme catalyzes an irreversible reaction and is part of a two-enzyme system with L-arginine dehydrogenase for the irreversible conversion of D-arginine to L-arginine.[27] Under nutrient-limiting conditions, the two-enzyme system enables *P. aeruginosa* to utilize D-arginine as the sole carbon and nitrogen source.[27] The physiological substrate that oxidizes the enzyme-bound flavin in *Pa*DADH is unknown, but the enzyme is unreactive with molecular oxygen.[26] *In vitro* kinetic studies have used phenazine methosulfate (PMS) as an electron acceptor. *Pa*DADH has a broad substrate specificity with D-amino acids, with D-arginine being the best substrate, as shown by a k_{cat}/K_m value of 10^6 M^{-1} s^{-1}.[26] A direct hydride ion transfer from the α-carbon atom of the deprotonated substrate to the enzyme-bound flavin oxidizes the substrate,[28] with a mechanism that is common to other flavin-dependent enzymes that oxidize amino acids, such as L-amino acid oxidase, D-amino acid oxidase, and monomeric sarcosine oxidase among others.[29] The atomic-resolution crystal structures of *Pa*DADH showed two conformations of active site loop L1,[26] with the side chain of Y53 forming hydrogen bonds with either T137 in the ligand-free conformation or the product's carboxylate in the product-bound enzyme, demonstrating the conformational flexibility of the enzyme.[26] In the product-bound enzyme, the side chain of Y249 forms a hydrogen bond with the product's carboxylate.[26] Interestingly, upon replacement of either Y53 or Y249 with phenylalanine, substrate binding is minimally affected, but flavin reduction becomes reversible, suggesting modulation of flavin reactivity by the tyrosine residues.[28] Replacement of Y249 with phenylalanine also yielded two enzyme populations, with an active enzyme variant containing yellow FAD (Y249F-y), which was characterized in a previous study, and an inactive enzyme variant harboring a green modified flavin cofactor (Y249F-g).[28]

We have carried out a biochemical, structural, and computational characterization of the yellow and green Y249F variant enzymes of *Pa*DADH. Our results show that a modified flavin cofactor, 6-OH-FAD, is responsible for the green-colored enzyme variant and establish that the side-chain hydroxyl of Y249 plays a vital role in the wild-type enzyme, preventing the formation of the 6-OH-FAD. Indeed, removing the Y249 hydroxyl changed the protein conformational landscape, altering the flavin electronic structure, thus modifying its reactivity.

EXPERIMENTAL PROCEDURES

Materials. D-Arginine, phenazine methosulfate, and PEG (3350, 5000, and 6000) were purchased from Sigma-Aldrich (St. Louis, MO). D-Alanine was obtained from Alfa Aesar (Wardhill, MA). Synthesized 6-OH-FAD was a kind gift of B. A. Palfey at the University of Michigan (Ann Arbor, MI). All of the other reagents used were obtained in their highest purity commercially available.

Enzyme Preparation. The Y249F enzyme was prepared by site-directed mutagenesis using the cloned wild-type gene pET20b(+)/PA3863 as a template, as described previously.[28] Expression and purification of the Y249F enzyme were described previously.[28] The purified Y249F-g and Y249F-y enzymes were stored in 20 mM Tris-HCl (pH 8.0) and 10% glycerol, at a concentration of 10 mg/mL. The expression, purification, and storage of the Y249F enzyme were also carried out in the absence of glycerol to improve the quality of the spectra in the MS-ESI analysis. The enzyme concentration was quantified using the Bradford method.[30,31] The ultraviolet−visible (UV−vis) absorption spectrum of the Y249F-y and Y249F-g enzymes was recorded with an Agilent Technologies model HP8453 PC diode array spectrophotometer equipped with a thermostated water bath.

Flavin Extraction and MS-ESI Analysis. The flavin cofactors were extracted from the Y249F-g and Y249F-y enzymes by treatment with ice-cold 7% (v/v) TCA for 30 min on an ice bath, followed by centrifugation at 10000*g* for 10 min to remove precipitated protein. The procedure was repeated on the supernatant to ensure the complete absence of protein. The extracted flavins were purified with an SCL-10A VP SHIMADZU HPLC instrument equipped with diode array detection. The stationary phase was a μBondapak C_{18} column (15 cm × 4.6 mm), the mobile phase consisted of H_2O and 0.01% TFA as solvent A and 5% acetonitrile and 0.01% TFA as solvent B. The flavin cofactors were loaded onto the column at 5% solvent B and eluted with a linear gradient from 5% to 100% solvent B developed in 60 min at a flow rate of 0.5 mL/min. FAD eluted at 21 min, and 6-OH-FAD at 24 min. The flavin cofactors extracted from the Y249F-y and Y249F-g enzymes were analyzed using mass spectrometry (MS) in the negative electrospray ionization (ESI) mode at the Mass Spectrometry Laboratory of Georgia State University. Accurate mass analysis was carried out using a Thermo Fisher Orbitrap Elite mass spectrometer equipped with an ESI source in negative ion mode. The samples were analyzed with an LC-MS profile without using a column and isocratic elution with 20% acetonitrile and 0.1% formic acid at a flow rate of 8 μL/min.

6-OH-FAD pK_a Determination. After extraction and purification by HPLC, the 6-OH-FAD was vacuum concentrated for ∼14 h and dissolved in 20 mM sodium phosphate and 20 mM sodium pyrophosphate (pH 6.0). The concentration of 6-OH-FAD was calculated using an ε_{422} of 19.6 mM^{-1} cm^{-1}.[32] The UV−vis absorption spectra of the 6-OH-FAD solution were recorded after serial additions of 1 M NaOH (1−10 μL), while the mixture was being stirred until the pH was incrementally changed. After each careful and slow addition of the base, the solution could equilibrate until no changes in the pH value or absorbance were observed, which typically required 2−3 min. The pH dependence of the absorbance at 585 nm was fit to eq 1

$$\mathrm{Abs}_{585\,nm} = \frac{C_L + C_H}{1 + 10^{pK_a - pH}} \quad (1)$$

where C_L and C_H are the pH-independent limiting values for the absorbance at 585 nm at low and high pH, respectively.

Lack of Reduction of the Y249F-g Enzyme with D-Arginine. A sample containing a mixture of the Y249F-y and Y249F-g enzymes (Y249F-yg) was prepared by gel filtration through a PD-10 desalting column (General Electric, Fairfield,

https://dx.doi.org/10.1021/acs.biochem.1c00054
Biochemistry 2021, 60, 711−724

CT) in 20 mM Tris-HCl (pH 8.7) at 25 °C. The Y249F-yg enzyme was incubated with 1.0 mM D-arginine in 50 mM Tris-HCl (pH 8.7) at 25 °C, and the UV−vis absorption spectrum was recorded before and after incubation with the amino acid substrate to establish whether the latter could reduce the Y249F-g enzyme. The Y249F-y enzyme present in the sample was used as an internal control because it was immediately reduced with the addition of D-arginine.

NMR Analysis. NMR experiments were conducted on a Bruker Avance 600 MHz spectrometer equipped with a 5 mm QXI ^{1}H (^{31}P, ^{13}C, ^{15}N) probe (Bruker, Billerica, MA). One-dimensional ^{1}H spectra were collected using the watergate W5 pulse sequence for water suppression.[33] Heteronuclear $^{1}H-^{13}C$ HSQC spectra were processed with a shifted squared sine bell multiplication in both dimensions (SSB = 2). A 100 ms mixing time was used for TOCSY spectra. Samples were prepared in 10 mM sodium phosphate (pH 7.0) and referenced to 4,4-dimethyl-4-silapentane-1-sulfonic acid (DSS) at 25 °C. Sample concentrations of HPLC-purified flavins ranged from 15 to 30 μM for 6-OH-FAD and ∼100 μM for FAD; commercial FAD and synthesized 6-OH-FAD sample concentrations were 300 μM.

Conversion of FAD to 6-OH-FAD in the Y249F-y Enzyme. The Y249F-y enzyme was incubated with 15 mM D-alanine in 20 mM Tris-HCl (pH 8.0) at 4 °C under aerobic conditions with constant stirring for 48 h. The flavin cofactors were extracted by treating the enzyme with 50% acetonitrile, 0.1% TCA, and centrifugation at 10000*g* to remove precipitated protein. The centrifugation step was repeated on the supernatant until no precipitation was observed. The resulting supernatant was vacuum concentrated for ∼1 h. Serial additions of 1 M NaOH were made to the samples after recording the initial UV−vis absorption spectrum at pH ∼2.0 to incrementally increase the pH to ∼10.0 and visualize the characteristic 540−800 nm band of the 6-OH-FAD.[32]

Incorporation of ^{18}O into 6-OH-FAD. A Y249F-y enzyme solution (15 μM, 1 mL) in 50 mM Tris-HCl (pH 8.0) was placed in a tonometer with a small stirring bar and a concentrated D-alanine solution in the side arm. The tonometer was made anaerobic by a 30-cycle treatment of flushing with oxygen-free argon and gas removal by applying vacuum. After the side arm solution was mixed with the enzyme, the resulting concentration of D-alanine was 15.0 mM. After mixing, the enzyme solution was incubated with constant stirring at 4 °C in the presence of $^{18}O_2$ gas by connecting a pressurized cylinder with the $^{18}O_2$ mixture to the tonometer. After 48 h, the protein was denatured with 50% acetonitrile previously cooled to −20 °C. The slurry was spun down at 10000*g* to remove precipitated protein, and the step was repeated on the supernatant until no precipitation was observed with centrifugation. The resulting supernatant was vacuum concentrated for ∼4 h. MS analysis for the extracted flavins was carried out on a Waters QTof micro mass spectrometer equipped with an ESI source in negative ion mode through a direct infusion at a flow rate of 5 μL/min. The ESI tuning settings were a capillary voltage of 3000, a sample cone voltage of 40, an extraction voltage of 1, a desolvation temperature of 100 °C, and a source temperature of 70 °C.

Enzyme Crystallization. Crystals of the Y249F-g and Y249-y enzymes were grown by the hanging-drop vapor diffusion method; 2 μL of a protein solution and 2 μL of a reservoir solution were mixed and equilibrated against 500 μL of a reservoir solution. Crystals of the Y249F-g enzyme were grown at room temperature using 50 mM Tris-HCl (pH 7.0), 10% glycerol, 13% (w/v) PEG 3350, and 6% (w/v) PEG 5000, as the well solution. Green pyramidal crystals were observed within 1 week and grew to a size of 0.2−0.3 mm^3 in 2 weeks. Crystals of the Y249F-y enzyme were grown at room temperature with 50 mM Tris-HCl (pH 7.0), 10% glycerol, 13% (w/v) PEG 3350, and 6% PEG 6000, as the well solution. Yellow crystals were observed within 1 week.

X-ray Data Collection and Processing. A single crystal of either the Y249F-g or Y249F-y enzyme was soaked for 2 s in the reservoir solution with 25% glycerol as a cryoprotectant and flash-frozen immediately in liquid nitrogen. Diffraction data were collected at 100 K on beamline 22-ID with an MX300HS detector of the Southeast Regional Collaborative Access Team (SER-CAT) at the Advanced Photon Source, Argonne National Laboratory. One hundred eighty images were collected at 1° oscillation per image with a crystal-to-detector distance of 190 mm, and exposure of 1.5 s per image. The data for Y249F-g and Y249F-y were processed using iMOSFLM and scaled with SCALA tools included in CCP4i Suite.[34,35]

Structure Solution and Refinement. The coordinates of wild-type *Pa*DADH [Protein Data Bank (PDB) entry 3NYE] were used for the molecular replacement step to obtain the initial phases for the Y249F-y and Y249F-g enzymes.[36] The tool Phaser found a unique solution in orthorhombic space group $P2_12_12_1$ with one molecule in the asymmetric unit for both Y249F-y and Y249F-g.[37] The crystal structures were refined with Phenix_refine.[38] Manual fitting and rebuilding were performed using the molecular graphics program Coot.[39] The 6-OH-FAD cofactor (6FA) coordinates were constructed using phenix_elbow and added during the refinement of the Y249F-g enzyme structure.[40] FAD was available in the PDB library and was added during refinement for the Y249F-y enzyme. Refined atomic coordinates and experimental structure factors were deposited in the Protein Data Bank (Y249-g, PDB entry 6PLD; Y249-y, PDB entry 6P9D). All structural figures were made using UCSF Chimera.[41]

Molecular Dynamics Simulations. Molecular dynamics (MD) simulations were carried out using the Amber16 suite of programs and AMBER ff14SB, a modified version of the force field of Cornell et al.[42,43] Initial coordinates of the systems were taken from the wild-type enzyme structure (PDB entry 3NYE) and the Y249F-y structure (PDB entry 6P9D).[36] The AmberTools xleap program was used to construct the appropriate system required for each MD simulation. The parameters of the FAD cofactor were obtained from the general AMBER force field (GAFF).[44] Each system was solvated in a periodic octahedron pre-equilibrated TIP3P[45,46] water box. The edges of the octahedron were at least 10 Å from the protein. All crystallographic water molecules were maintained. The systems were then neutralized using Na^+ or Cl^- counterions and equilibrated to 300 K and 1 bar.

A detailed equilibration protocol can be found in ref 47. More specifically, the systems were energy minimized for 5000 steps with the positions of the protein atoms held by harmonic constraints. Five rounds of energy minimization were performed, where the force constant of the positional constraints was gradually decreased from 500 to 0 kcal mol^{-1} $Å^{-2}$. The system was heated from 100 to 300 K for 500 ps using a 1 fs time step and positional constraints on the protein atoms, and the temperature was maintained using the Langevin thermostat with a collision frequency of 1.0 ps^{-1} under the

https://dx.doi.org/10.1021/acs.biochem.1c00054
Biochemistry 2021, 60, 711−724

NVT ensemble. Five rounds of heating were performed, where the force constant of restraint was set to 500, 300, 100, 50, or 5 kcal mol^{-1} $Å^{-2}$. A final equilibration step was carried out for 1 ns with a time step of 2 fs and no positional constraints under the *NPT* ensemble at a constant temperature of 300 K and a constant pressure of 1 bar using the Monte Carlo barostat with a coupling constant of 1.0 ps. All production simulations were carried out for 1.2 μs. The first 200 ns was considered to be an extension of the equilibration phase, and the last 1.0 μs was used for analysis. The particle mesh Ewald (PME) summation[48] was used to evaluate long-range electrostatic interactions. A 9 Å cutoff was used for all short-range nonbonded interactions. All bonds involving hydrogen atoms were constrained using the SHAKE algorithm.[49] The snapshots of the trajectories were saved every 1 ps (500 steps).

Molecular Dynamics Simulations with O_2 Molecules. Additional MD simulations of the wild-type and mutant enzymes with O_2 molecules were carried out for 1.2 μs, similar to the description above. In addition to the procedure presented above, four O_2 molecules were added randomly to the solution around the protein molecule.

Principal Component Analysis (PCA). PCA was performed using the CPPTRAJ program[50] in the Amber16 suite of programs on the MD simulation trajectories. The backbone atoms for all of the snapshots were structurally superposed. The eigenvectors and eigenvalues were calculated from the covariance matrix characterizing the internal motions of all of the heavy atoms of the active site residues. Each eigenvector represents a principal component (PC), and the associated eigenvalue describes the structural variation captured by the PC. The top two PCs (PC1 and PC2) captured the largest structural variance and were used to project back on the simulation trajectories to represent the conformational dynamics for the active sites of the wild type and mutant.

Hybrid Quantum Mechanical/Molecular Mechanical (QM/MM) Calculations. Hybrid QM/MM calculations were carried out for the wild type and for different conformations of the Y249F-y enzymes to determine the spin densities on the atoms of the flavin isoalloxazine moiety. Specifically, the protocol used is based on the Average Solvent Electrostatic Environment-Free Energy Gradient (ASEC-FEG) approach used previously for rhodopsins,[51] which was extended here to flavoproteins. Briefly, the ASEC-FEG approach computes quantum mechanical properties of the cofactor in a superposition of several protein conformations instead of using a single protein structure. ASEC-FEG, therefore, accounts for the effect of local protein flexibility on the quantum mechanically computed properties. The ASEC-FEG QM/MM models were constructed by dividing each enzyme into three subsystems, labeled QM, MM_1, and MM_2.

The QM subsystem, shown in Figure 1 with shaded atoms, was described using quantum mechanics and included all atoms of the reduced anionic lumiflavin moiety, up to the link atom (LA). The LA lies at the frontier between the QM and MM_1 subsystems and is a hydrogen atom that caps the valency created by breaking a C_{QM}–C_{MM1} bond.[52] The position of the LA was restrained according to the Morokuma scheme, such that it remains colinear with the C_{QM}–C_{MM1} bond.[53] The MM_1 subsystem, also shown in Figure 1, includes some of the $FADH^-$ ribityl atoms near the LA. The MM_1 subsystem was treated using molecular mechanics with the AMBER99sb[54,55] force field and is optimized along with the QM subsystem

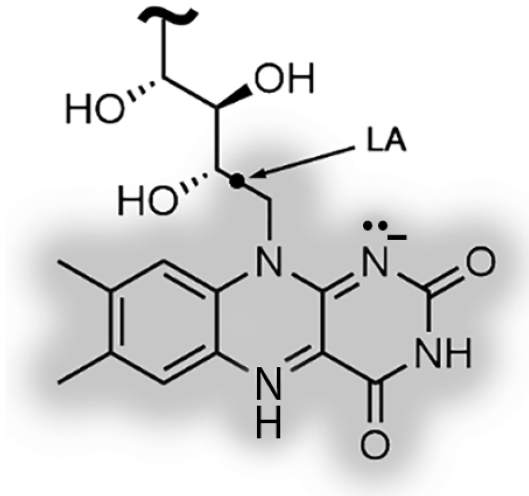

Figure 1. Division of $FADH^-$ into QM (shaded atoms) and MM atoms. The frontier valency is saturated by a hydrogen link atom (LA).

during QM/MM optimization steps of the protocol. The MM_2 subsystem includes all other atoms of the $FADH^-$, the *Pa*DADH protein, and surrounding water molecules and ions, i.e., all atoms not shown in Figure 1. The MM_2 subsystem was treated with molecular mechanics with the AMBER99sb[54,55] and TIP3P[56] force fields for the protein and water molecules, respectively, and was sampled to generate the ASEC configurations.

QM/MM calculations were performed for wild-type *Pa*DADH and for different conformational substates of the Y249F-y enzyme obtained from the 1000 ns MD simulations discussed in the previous section using the following protocol. These proteins were resolvated in a 10 nm cubic water box with 17 Na^+ counterions to ensure a globally neutral system.

Periodic boundary conditions were used to avoid boundary effects. Short MD simulations were then performed for the MM_2 subsystem while keeping the QM and MM_1 subsystems frozen to generate the ASEC configurations for the proteins while maintaining each system in the same substate sampled by the long MD simulations. Specifically, the sampling MD simulations were run for a total of 11.3 ns, just long enough to sample local side-chain rotations and flexibility within each protein substate. Those include a 0.3 ns heating simulation, in which the temperature was slowly increased from 0 to 300 K, a 1 ns thermalization in the *NPT* ensemble to equilibrate the volume of the system, a 5 ns *NVT* equilibration run, and a 5 ns production run. The GROMACS code[57] was used for these MD simulations. The MD simulations were used to select 100 statistically uncorrelated snapshots to generate an "ASEC" configuration of the MM_2 subsystem, which is a superposition of the 100 protein configurations with scaled charges and van der Waals parameters such that the QM/MM interaction energy is computed under conditions mimicking thermodynamic equilibrium conditions.[51,58] The QM and MM_1 subsystems were then optimized within the resulting ASEC environment. The QM/MM calculations were performed using the MOLCAS[59]/TINKER[60] QM/MM interface.[61] QM/MM geometry optimizations were performed using the CASSCF/ANO-L-VDZP[62,63] level of theory with 14 orbitals and 18 electrons (for $FADH^-$) or 17 electrons (for FADH• or FAD^-•) included in the active space. The optimized geometry

https://dx.doi.org/10.1021/acs.biochem.1c00054
Biochemistry 2021, 60, 711−724

was used to obtain updated charge parameters for the cofactor using the RESP protocol,[64] and another MD simulation was performed to obtain a new ASEC configuration based on the QM/MM-optimized geometry and charges. The iterative process described above was used to obtain a self-consistent $QM/MM_1/MM_2$(ASEC) system.

The optimized QM/MM structures with the updated ASEC configurations were then used to generate four models for wild-type *Pa*DADH and the different conformational substates Y249F-y. The resulting four sets of data represent different sets of assumptions to accommodate all possible mechanisms and time scales of proton movements in the oxidative reaction catalyzed by the enzyme, which was not known; these were as follows.

FADH• at Equilibrium. This data set considers the possibility that the reduced $FADH^-$ state is oxidized to a neutral FADH• that is long-lived enough for the QM/MM environment to equilibrate around it. In this case, the MM_2(ASEC) and QM/MM_1 optimizations and spin densities are consistently generated for FADH•.

FADH• Not at Equilibrium. This data set considers the possibility that the reduced $FADH^-$ state is oxidized to a neutral FADH•, but that FADH• reacts instantaneously with O_2. In this case, the MM_2(ASEC) is generated for $FADH^-$ but the QM/MM_1 optimizations and spin densities are computed for FADH•; i.e., we assumed the protein environment would not have time to equilibrate before FADH• reacts.

FAD^-• at Equilibrium. This data set considers the possibility that the reduced $FADH^-$ state is oxidized to an anionic flavosemiquinone, i.e., FAD^-•, that is long-lived enough for the QM/MM environment to equilibrate around it. In this case, the MM_2(ASEC) and QM/MM_1 optimizations and spin densities are consistently computed for FAD^-•.

FAD• Not at Equilibrium. This data set considers the possibility that the reduced $FADH^-$ state is oxidized to a FAD^-• that reacts instantaneously with O_2. In this case, the MM_2(ASEC) is generated for $FADH^-$ but the QM/MM_1 optimizations and spin densities are computed for FAD^-•; i.e., we assumed the protein environment would not have time to equilibrate before FAD^-• reacts.

The Mulliken spin densities were computed using the same CASSCF/ANO-L-VDZP/AMBER99sb level of theory used for the optimization. The spin density calculations were also repeated using unrestricted B3LYP[65]/ANO-L-VDZP calculations for comparison. UB3LYP has been successfully used to model several properties of flavin in different redox states,[66,67] while the CASSCF/AMBER QM/MM approach is widely used to perform multiconfigurational electronic structure calculations of protein-bound molecules.[68] Both UB3LYP and CASSCF calculations showed the same trends in spin densities, so only the CASSCF values are reported in the results.

RESULTS

UV−Vis Absorbance of the Y249F-y and Y249F-g Enzymes. The Y249F variant of *Pa*DADH was isolated in three fractions with yellow, light green, and green colors (Figure 2A, inset) that could be separated using a DEAE-Sepharose column. The yellow enzyme, Y249F-y, was active, contained FAD, and was previously characterized.[23] The Y249F-y enzyme showed a UV−vis absorption spectrum at pH 8.7 with maximal absorbance at 370 and 445 nm and no absorbance above 540 nm (Figure 2A).

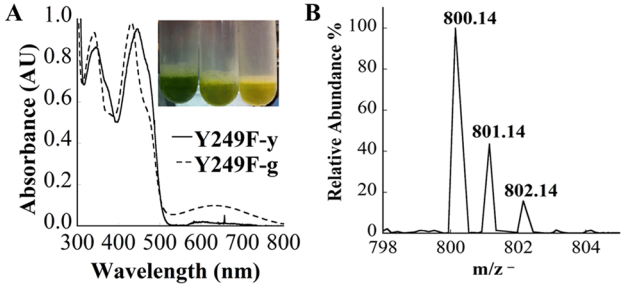

Figure 2. Spectroscopic characterization of the green flavin. (A) UV−vis absorption spectra of the Y249F-y (solid curve) and Y249F-g (dashed curve) enzymes were acquired at pH 8.7. The inset shows the enriched green inactive fraction Y249F-g, a mixture of the Y249F-y and Y249F-g enzyme fractions (Y249F-yg), and the enriched Y249F-y fraction after ion-exchange chromatography. (B) MS-ESI spectrum of the green flavin extracted from the Y249F-g enzyme in negative ion mode, showing an m/z (−) value at 800.14 amu and the naturally abundant isotopic pattern.

The green enzyme, Y249F-g, showed a broad band in the range of 540−800 nm and maximal absorbance at 350 and 429 nm (Figure 2A). The light green enzyme contained a mixture of yellow and green enzymes (Y249F-yg).

MS-ESI Analysis of 6-OH-FAD. To establish the atomic composition of the green modified flavin in the Y249F-g enzyme, the enzyme was denatured, and the extracted flavin was subjected to mass spectrometry. An MS-ESI analysis showed an m/z (−) value of 800.14 amu for the extracted green modified flavin (Figure 2B), consistent with an extra O atom being present on FAD. A control experiment of the yellow flavin extracted from the Y249F-y enzyme yielded an m/z (−) value of 784.05 amu (data not shown), in agreement with the expected value of 784.55 amu for FAD. These data are consistent with the green flavin being a hydroxylated form of FAD[69] but do not establish the site of modification on the flavin cofactor.

Determination of the pK_a Value of 6-OH-FAD. The pK_a value of the extracted green modified flavin was determined in a pH titration of the UV−vis absorption spectrum (Figure 3A). A plot of the absorbance at 585 nm versus pH yielded a pK_a value of 7.1 ± 0.1 (Figure 3A, inset), which agrees with previous data on proton-exchangeable equilibria of 6- or 9-OH-FAD in bulk solution.[32,70,71]

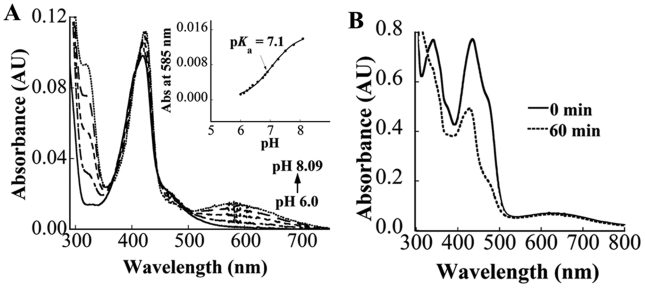

Figure 3. Spectroscopic characterization of the green flavin. (A) UV−vis absorption spectra of the green flavin extracted from the Y249F-g enzyme as a function of pH, with the inset showing the determined pK_a value. For the sake of clarity, only select spectra are shown between pH 6.0 and 8.1. (B) Functional assessment of the Y249F-yg enzyme containing a mixture of FAD and 6-OH-FAD: oxidized enzyme before (solid curve) and after incubation for 60 min with 1 mM D-arginine (dotted curve).

https://dx.doi.org/10.1021/acs.biochem.1c00054
Biochemistry 2021, 60, 711−724

Lack of Activity of the Y249F-g Enzyme. To establish whether the 6-OH-FAD could be reduced in the active site of *Pa*DADH, the enzyme containing a mixture of both 6-OH-FAD and FAD, i.e., Y249F-yg, was incubated with 1.0 mM D-arginine at pH 8.7, and the UV−vis absorption spectrum was acquired. The variant enzyme containing both flavins was chosen because it provided an internal standard, i.e., the FAD., which was expected to be reduced in the substrate's presence. The absorbance at 445 nm of the Y249F-yg enzyme immediately decreased upon incubation of the enzyme with the substrate (Figure 3B), consistent with the enzyme with FAD being active. Instead, the long-wavelength band in the 540−800 nm region of the spectrum persisted after incubation with D-arginine (Figure 3B), indicating that the amino acid substrate could not reduce the variant enzyme containing the green modified flavin. Thus, the enzyme with the green modified flavin was not active, in agreement with previous results in other systems showing that enzymes containing 6-hydroxylated flavins retain low to no activity with their physiological substrates.[32,72−75]

NMR Analyses of 6-OH-FAD. The green flavin extracted from the Y249F-g enzyme was subjected to NMR analysis to establish whether the extra OH group was on the flavin C6 or C9 atom. A synthesized 6-OH-FAD standard and commercially available FAD were also analyzed for reference. Three aromatic peaks are observed in the ^{1}H NMR spectra of the extracted green flavin sample (at 7.8 ppm, at 8.35 ppm, and a novel resonance at 6.75 ppm) and are identical to those of the synthesized 6-OH-FAD sample (Figure 4A). The adenosine resonances were identified via comparison to the FAD standard, leaving the resonance at 6.75 ppm corresponding to a proton on the isoalloxazine ring (Figure 4B). Analysis of TOCSY spectra obtained from the synthesized 6-OH-FAD and the green flavin extracted from the Y249F-g sample reveals identical coupling between the aromatic peak at 6.75 ppm and the isoalloxazine methyl proton at 2.4 ppm (Figure 4C,D). Thus, by direct comparison with standards, the ^{1}H NMR, TOCSY, and HSQC analyses established that the green flavin's modification was on the C6 atom and not the C9 atom.

Conversion of FAD to 6-OH-FAD in the Y249F-y Enzyme. The 6-OH-FAD in *Pa*DADH could be formed through an ionic mechanism in which the flavin hydroquinone is a required intermediate, as previously proposed for trimethylamine dehydrogenase.[76] To determine whether the hydroquinone was required to convert FAD to 6-OH-FAD in the active site of *Pa*DADH, the Y249F-y enzyme was reduced aerobically with 15 mM D-alanine at pH 8.0 and 4 °C, and the resulting UV−vis absorption spectrum was acquired. As shown in Figure 5A, the aerobic treatment of the enzyme with the D-alanine resulted in FAD's conversion to 6-OH-FAD. An MS-ESI analysis of the modified flavin after extraction from the enzyme confirmed the formation of the 6-OH-FAD, with an m/z (−) value of 800.19 amu in the mass spectrometry spectrum (Figure 5B). In the absence of D-alanine, there were no changes in the absorption maxima of the enzyme-bound FAD at 377 and 449 nm (Figure 5A). Thus, the flavin hydroquinone produced in the substrate-driven reduction of the flavin with D-alanine could be a possible intermediate that allows for the *in vitro* formation of 6-OH-FAD from FAD in the active site of the Y249F-y enzyme.

The aerobic incubation of the Y249F-y enzyme with 15 mM D-alanine was repeated in an atmosphere enriched with $^{18}O_2$ gas to establish whether the O atom incorporated in the 6-OH-FAD originated from molecular O_2. In the MS-ESI spectrum of the extracted flavin reduced with D-alanine in the presence of $^{18}O_2$ gas, the relative intensity of the peak with an m/z (−) value of 802.16 amu increased as compared to that treated with atmospheric O_2 gas, consistent with the incorporation of a ^{18}O atom in the newly formed 6-OH-FAD. Thus, the O atom of the 6-OH-FAD originated from molecular O_2.

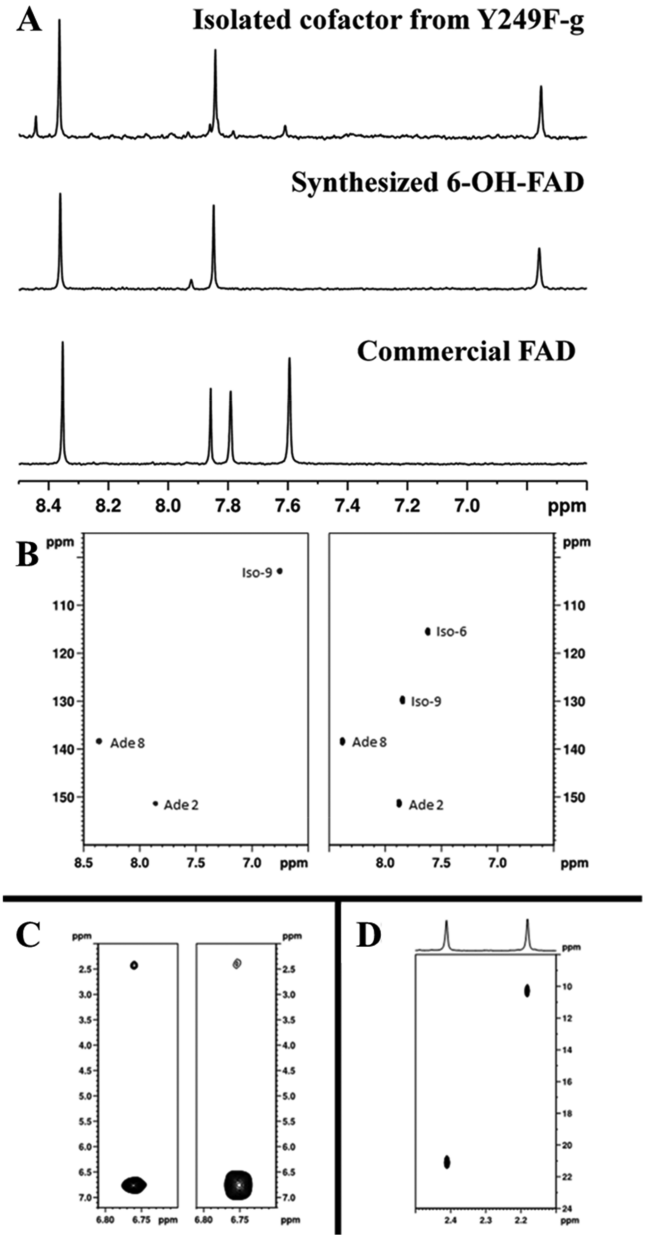

Figure 4. ^{1}H NMR and HSQC spectra of the modified flavin. (A) Comparison of ^{1}H NMR spectra of the green flavin isolated from the Y249F-g enzyme (top), synthesized 6-OH-FAD (middle), and FAD (bottom). ^{1}H NMR spectra of the extracted flavin and a chemically synthesized 6-OH-FAD yielded identical chemical shifts, confirming the modification was at the C6 position of the isoalloxazine moiety of FAD. (B) HSQC spectra of aromatic regions of synthesized 6-OH-FAD (left) and FAD (right). (C) Slices from TOCSY spectra showing coupling between position 9 of the isoalloxazine ring and the adjacent methyl protons (left, synthesized; right, HPLC-purified). (D) HSQC spectrum of 6-OH-FAD methyl protons. The separation between methyl protons is 0.24 ppm.

https://dx.doi.org/10.1021/acs.biochem.1c00054
Biochemistry 2021, 60, 711−724

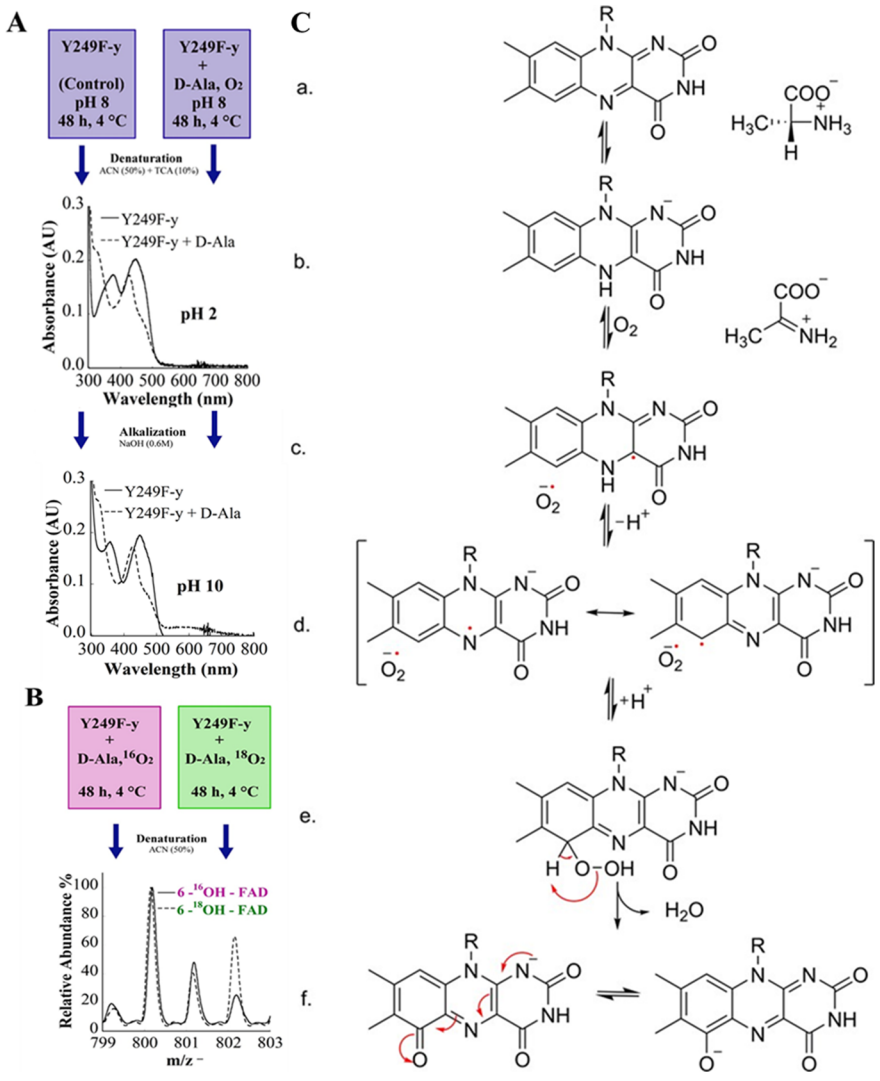

Figure 5. Conversion of FAD to 6-OH-FAD in the Y249F-y enzyme. (A) The Y249F-y enzyme was incubated for 48 h in the presence or absence of 15 mM D-alanine at pH 8.0 and 4 °C (top). UV−vis absorption spectra of the isolated cofactors after the treatment of the enzymes with acidified 50% acetonitrile and centrifugation to remove denatured protein at pH 2.0 (middle) and alkalization with 0.6 M NaOH (bottom). (B) MS-ESI spectra of the extracted cofactors after aerobic incubation of the Y249F-y enzyme with 15 mM D-alanine in natural and $^{18}O_2$ gas-enriched atmospheres after extraction with 50% acetonitrile. (C) Proposed mechanism for hydroxylation of FAD in the active site of the Y249F-y enzyme. The description is given in the text.

Proposed Mechanism for the Formation of 6-OH-FAD. On the basis of the requirement of a flavin hydroquinone and the observation that the O atom incorporated in the 6-OH-FAD originated from O_2, a mechanism for the formation of 6-OH-FAD could be proposed (Figure 5C). Briefly, the enzyme-bound FAD is initially reduced by D-alanine before reacting with O_2 via a single-electron transfer generating a neutral flavosemiquinone and superoxide anion; the two radical species collapse with the formation of a C6-peroxo-FAD, which after elimination of water yields 6-OH-FAD. If one assumes rapid equilibration of protons, an anionic flavosemiquinone could also be considered before forming the 6-peroxo-FAD, as illustrated by the species in brackets in Figure 5C. Irrespective of the ionization state of the flavosemiquinone, the proposed mechanism suggests there is an increased tendency for O_2 to react at C6 of the flavin in the Y249F mutant relative to the wild-type system, where such a reaction does not occur. One possibility is an enhanced reactivity at C6 of flavin in Y249F, while another possibility is easier O_2 access to the active site. We tested both hypotheses using MD and QM/MM calculations (see below).

X-ray Crystal Structures of the Y249F-g and Y249F-y Enzymes. The high-resolution X-ray crystal structures of the Y249F enzymes with either 6-OH-FAD or FAD were independently determined in space group $P2_12_12_1$. The space group was the same as that previously seen for the structure of wild-type *Pa*DADH.[36] The structure of the Y249F-g enzyme with 6-OH-FAD (PDB entry 6PLD) was refined to an *R* factor of 0.16 and a resolution of 1.55 Å and that of the yellow Y249F-y enzyme with FAD (PDB entry 6P9D) to an *R* factor of 0.13 and a resolution of 1.33 Å. The crystallographic and refinement statistics are listed in Table 1.

Superposition of the backbone atoms of either the Y249F-g or the Y249F-y enzyme with the structure of the wild-type enzyme previously determined (PDB entry 3NYE) yielded root-mean-square deviation (RMSD) values of ≤0.38 Å over 375 polypeptide backbone atoms (Figure 6). The structure of the Y249F-g enzyme lacked electron density on the C4 atom of

https://dx.doi.org/10.1021/acs.biochem.1c00054
Biochemistry 2021, 60, 711−724

Table 1. Data Collection and Refinement Statistics for X-ray Crystal Structures

	*Pa*DADH Y249F-g (PDB entry 6PLD)	*Pa*DADH Y249F-y (PDB entry 6P9D)
	Data Collection[a]	
space group	*P*212121	*P*212121
cell dimensions		
a, *b*, *c* (Å)	59.78, 73.91, 76.98	60.10, 74.03, 77.19
α, *β*, *γ* (deg)	90.00, 90.00, 90.00	90.00, 90.00, 90.00
resolution (Å)	59.78−1.55 (1.58−1.55)	59.74−1.34 (1.58−1.34)
R_{merge}	0.103 (0.488)	0.020 (0.200)
$I/\sigma I$	10.6 (3.2)	17.2 (3.6)
completeness (%)	96.1 (93.4)	99.4 (96.9)
redundancy	7.0 (6.5)	2.0 (2.0)
	Refinement	
resolution (Å)	39.8−1.55	37.01−1.33 (1.38−1.33)
no. of reflections	53764	79364 (7694)
R_{work}/R_{free}	0.16/0.20	0.13/0.17
no. of atoms	3578	3770
protein	3079	3286
ligand/ion	109	95
water	390	389
B-factor (Å^2)	17.0	16.62
protein	16.20	14.50
ligand/ion	21.60	23.44
water	28.28	32.80
root-mean-square deviation		
bond lengths (Å)	0.006	0.006
bond angles (deg)	1.178	1.23

[a]Values in parentheses are for the highest-resolution shell.

F249, as expected due to the mutation of Y249 to phenylalanine. Additional electron density was present on the flavin C6 atom (Figure 7A), consistent with 6-OH-FAD in the Y249F-g enzyme. In contrast, the structure of the Y249F-y enzyme lacked electron density on both the C4 atom of F249 and the flavin C6 atom, consistent with the mutation of Y249 to phenylalanine and the presence of unmodified FAD.

The Y249F-g and wild-type enzymes shared identical conformations of all of the active site residues and flavin (Figure 7B). In the Y249F-y enzyme, instead, the conformations of both the guanidino group of R222 and R305 could be modeled only between 60% and 80% occupancy (Figure 7C,D). This enzyme conformation was labeled conformation A. The guanidino group of R222 was also present in an alternative conformation that could be modeled for 40% occupancy (Figure 7C,D), which was labeled conformation B. Although residual electron density for the side chain of R305 was observed at lower σ levels, a unique alternative conformation of the guanidino group of R305 could not be modeled with confidence. Residual electron density for the FAD was also observed in the Y249F-y enzyme, but again a unique alternative conformation could not be modeled with confidence (Figure 7C). Thus, the FAD and the side chains of R222 and R305 in the Y249F-y enzyme appeared to be mobile. A similar case of FAD being in multiple conformations was previously observed in the crystal structure of an enzyme variant of *p*-hydroxybenzoate hydroxylase, in which Y222 was replaced with phenylalanine.[77]

MD Simulations. To probe whether replacement of Y249 with phenylalanine was responsible for the unique conformational substate seen in the X-ray structure of the Y249F-y enzyme, i.e., conformation B, MD simulations were carried out on the wild type and the two conformations of the Y249F-y enzyme. Unrestrained MD simulations were carried out for 1.2 *μ*s to generate an ensemble of accessible conformations of the Y249F-y and wild-type enzymes.[78] PCA showed that the Y249F-y and wild-type enzymes share most of the conformational landscape, i.e., conformation A (Figure 8). The Y249F-y enzyme had an extra conformational substate in the PCA involving the guanidino groups of R222 and R305 and the FAD that was not available to the wild-type enzyme (Figures 8 and 9). Thus, the replacement of Y249 with phenylalanine permits a conformational substate in the mutant enzyme that is impeded in the wild-type enzyme; i.e., conformation B is available to the Y249F enzyme but not wild-type *Pa*DADH.

O_2 Localization in the Active Site. To establish whether the effect of the single-point mutation unlocking a transient conformational state in the protein was due to altered localization of O_2 to the flavin C6 atom, additional MD simulations with O_2 molecules were carried out. O_2 molecules were able to freely access the active site of the wild-type and mutant enzymes. There was no significant difference in the localization of O_2 around the flavin C6 atom in the Y249F-y and wild-type enzymes. The replacement of Y249 with phenylalanine yielded minimal, if any, steric control of the formation of 6-OH-FAD in the active site of *Pa*DADH, suggesting that the modification was due to the change in the electronic configuration of the flavin.

Hybrid QM/MM Electron Spin Density Flavin Computations. To determine whether the transient conformational substate unlocked in the Y249F-y enzyme by the single-point mutation yielded an altered chemical reactivity of the flavin, hybrid QM/MM calculations were used to model the electron spin density of the flavin in conformation A and conformation B of the Y249F-y enzyme and the wild-type enzyme. As described in the QM/MM methodology section, multiple models were considered to allow for both the neutral flavosemiquinones, anionic flavosemiquinones, and the protein equilibrated before and after electron transfer. The latter requirements allowed for either rapid formation of 6-peroxo-FAD after superoxide formation or sufficiently slow reactivity to allow protein equilibration, because this was not experimentally established and was beyond the scope of this study. As shown in Table 2, the QM/MM analysis showed that the flavin C6 atom in the Y249F-y enzyme's conformation B had a higher spin density than in conformation A, irrespective of protein equilibration or the flavosemiquinone ionization's state. The same result was obtained for UB3LYP spin density calculations. Thus, the replacement of Y249 with phenylalanine is associated with a change in protein dynamics, unlocking a conformational substate with an altered FAD reactivity, which likely results in the formation of 6-OH-FAD in the active site of *Pa*DADH.

DISCUSSION

The biochemical, structural, and computational investigation presented here demonstrates that Y249 in *Pa*DADH exerts a tight control on the reactivity of flavin by limiting the ensemble of conformational substates that could be otherwise sampled by the protein in the absence of the Y249 hydroxyl group. The X-ray structures of the mutant enzyme before and after the

https://dx.doi.org/10.1021/acs.biochem.1c00054
Biochemistry 2021, 60, 711−724

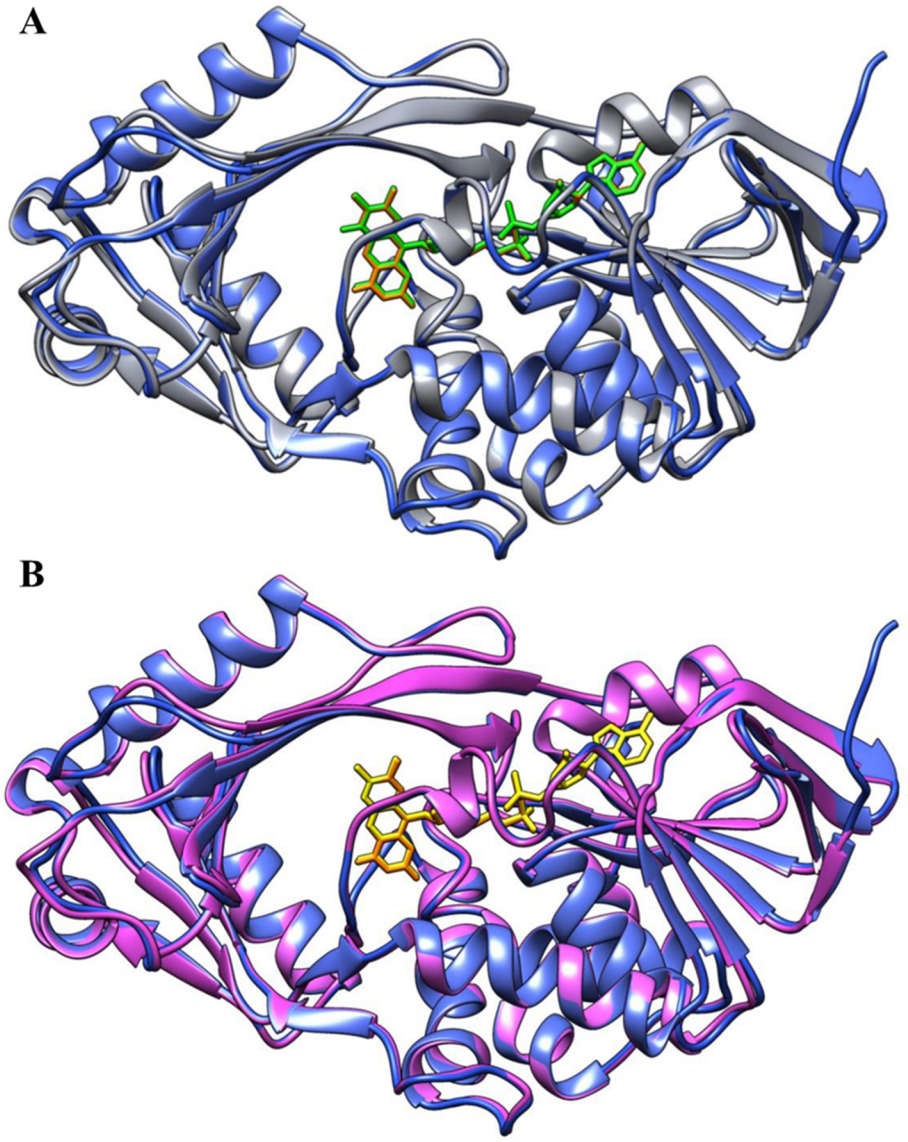

Figure 6. Overall structure of the Y249F-g and Y249F-y enzymes. (A) Overlay of the Y249F-g (gray) and wild-type (purple) structures, showing similar overall folds, with RMSD values of 0.36 Å over 375 polypeptide backbone atoms. (B) Overlay of the Y249F-y (pink) and wild-type (purple) structures, showing similar overall folds, with RMSD values of 0.38 Å over 375 polypeptide backbone atoms.

formation of 6-OH-FAD, i.e., the Y249F-y enzyme in conformation A and the Y249F-g enzyme, are identical to that of the wild-type enzyme. The crystal structure does, however, suggest an alternative conformation for some flexible residues but does not entirely explain what features may alter the reactivity of the flavin. However, MD simulations demonstrate that, upon removal of the Y249 hydroxyl by mutation to phenylalanine, the protein samples a new conformational landscape not available to the wild-type enzyme, i.e., Y249F-y conformation B. MD simulations also indicate no difference in O_2 localization in the mutant and wild-type enzymes, while hybrid QM/MM spin density calculations indicate that conformation B has altered flavosemiquinone reactivity. This suggests that Y249F-g is formed only in the transient conformation B substate of Y249F, which is not observed in the wild-type protein.

Proteins are dynamic and sample a wide range of conformations to stabilize transition states, control substrate access to and product release from the active site, and provide proper electrostatic interactions for catalysis and substrate binding.[79] Any perturbation to the existing ensemble of conformations can severely impact enzyme activity, as demonstrated in *Pa*DADH, where a point mutation removing an O atom from the side chain of an active site residue modifies protein dynamical pathways and leads to altered cofactor reactivity. This conclusion further expands conclusions from previous studies of *Ec*DHFR showing that mutations affect the enzyme's ability to sample specific conformations associated with the hydride transfer reaction catalyzed by the enzyme.[11,79] The results presented in this study suggest that the dynamics of enzymes orchestrate their function due to the highly optimized interactions and coupled motions between the different residues that can be altered with the slightest change in the amino acid sequence.

Apart from the side-chain conformations and protein motions, flavin dynamics also have an essential role in substrate binding and catalysis.[77] The ribityl moiety and the isoalloxazine ring are the most mobile portions of flavins and

https://dx.doi.org/10.1021/acs.biochem.1c00054
Biochemistry 2021, 60, 711−724

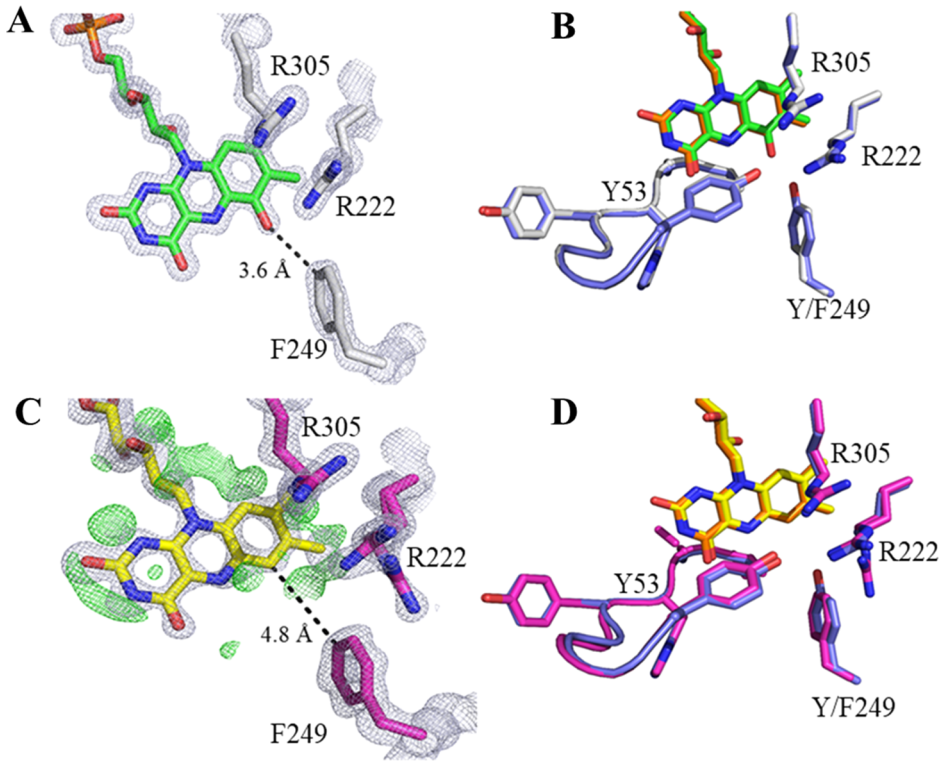

Figure 7. Active sites of the Y249F-y and Y249F-g enzymes. (A) Electron density map ($2F_o - F_c$ contoured at 2σ) of the Y249F-g enzyme, showing 6-OH-FAD. (B) Active site overlay of Y249F-g (gray) and wild-type *Pa*DADH (purple), demonstrating no changes in the active site. (C) Electron density map ($2F_o - F_c$ contoured at 1.3σ, in gray, and $F_o - F_c$ contoured at 3.0σ, in green) of the flavin and electron density map ($2F_o - F_c$ contoured at 1.3σ, in gray) of R305, R222, and F249 in the active site of the Y249F-y enzyme. (D) Active site overlay of the Y249F-y (pink) and wild-type *Pa*DADH (purple) demonstrating two major conformations for the side chain of R222.

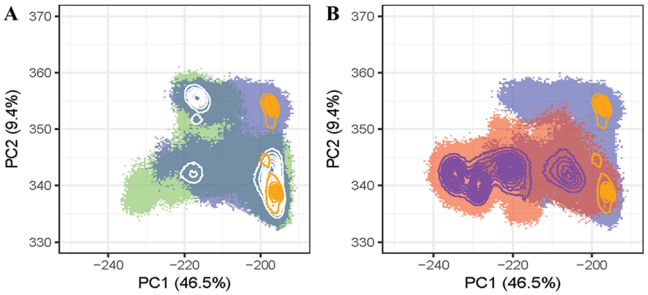

Figure 8. Conformational flexibility of the active site in the Y249F-y variant. (A) Principal component analysis as a scatter plot for wild-type *Pa*DADH (purple) and Y249F-y conformation A (green), demonstrating significant overlap between wild-type *Pa*DADH and Y249F-y conformation A. The concentric circles in orange indicate the highest-density areas for the wild type and in white for Y249F-y conformation A. (B) Principal component analysis as a scatter plot for wild-type *Pa*DADH (purple) and Y249F-y conformation B (red) demonstrating overlap between the Y249F-y conformation B to a lower degree, compared to Y249F-y conformation A and a novel conformational state in conformation B. The concentric circles in orange indicate the highest-density areas for the wild type and purple for Y249F-y conformation B.

can be stabilized by hydrogen bonding interactions.[80] *p*-Hydroxybenzoate hydroxylase was one of the first enzymes for which structural evidence for a mobile flavin existing in two conformations, namely, "in" and "out", was established in a Y222 to phenylalanine enzyme variant.[81] In contrast to the wild-type enzyme, the flavin in *p*-hydroxybenzoate hydroxylase prefers the "out" conformation, with the isoalloxazine ring away from the substrate binding site in the Y222F enzyme, with R220 providing a significant stabilizing interaction to maintain the "out" conformation.[77] Interestingly, in both *Pa*DADH and *p*-hydroxybenzoate hydroxylase, protein dynamics is altered when an active site tyrosine is replaced with phenylalanine, although a rationale is not immediately clear. Perhaps nature has exploited the ability of the tyrosine's hydroxyl side chain to act concomitantly as both a hydrogen bond donor and a hydrogen bond acceptor to firmly limit the ensemble of conformational substates potentially available to the protein. More recently, studies of enzymes like *N*-hydroxylases/monooxygenase, tetracycline resistance enzymes, and other flavin monooxygenases have focused on elucidating the role of cofactor dynamics and how it can be coupled to substrate binding and catalysis.[82−85]

Cofactor versatility and the fine-tuning of the cofactor reactivity are other aspects that dictate enzyme activity.[86] The effect of the protein microenvironment on the flavin cofactor is evident in Y249F-y variant conformation B, where a higher spin density on the C6 position of the flavosemiquinone species was observed. Another flavin-dependent enzyme in which the microenvironment's effect can be demonstrated on the flavin cofactor is trimethylamine dehydrogenase (TMADH). A substrate-assisted mechanism proposed for the formation of 6-OH-FAD in Y249F-y was also proposed for the C30 to alanine variant of TMADH.[76] The FMN cofactor in wild-type TMADH is covalently attached to the protein through a 6-*S*-cysteinyl bond, and upon mutation of the cysteine responsible for covalent attachment, the FMN undergoes a substrate-assisted reduction and reacts with molecular oxygen to form 6-hydroxy-FMN.[76,87] Interestingly,

https://dx.doi.org/10.1021/acs.biochem.1c00054
Biochemistry 2021, 60, 711−724

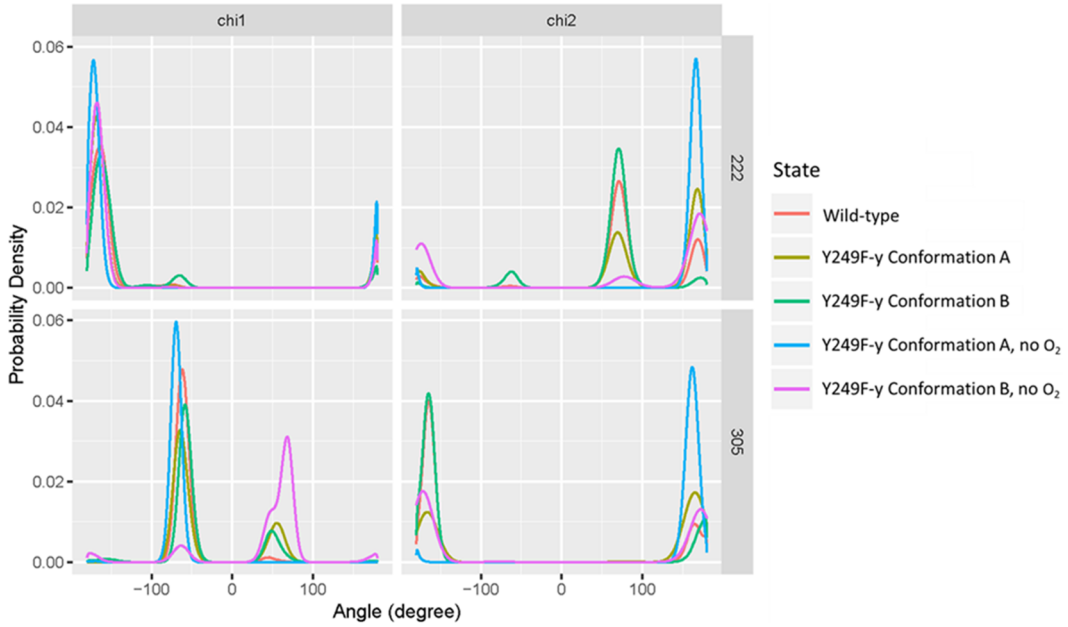

Figure 9. Side-chain flexibility for R222 and R305. Probability distribution plot for the side-chain dihedral angles for arginines 222 and 305. The plot demonstrates the frequency of dihedral angle space accessed at χ_1 and χ_2 of R222 and R305 for WT *Pa*DADH, conformations A and B of Y249F-y, in the presence and absence of O_2.

Table 2. QM/MM Spin Density Calculations for the Flavin C6 Atom

flavin species	WT	conformation A	conformation B
FADH•, equilibrium[a]	0.017	0.014	0.035
FADH•, non-equilibrium[b]	0.017	0.015	0.038
FAD^-•, equilibrium[a]	0.107	0.128	0.136
FAD^-•, non-equilibrium[b]	0.049	0.107	0.144

[a]The equilibrium models assume that the species is long-lived enough to allow equilibration of the protein environment and sampling of the configurational space around the flavosemiquinone. [b]The non-equilibrium models assume that the flavosemiquinone reacts instantaneously, i.e., with the protein in a frozen state in the ASEC configuration corresponding to the fully reduced anionic system.

the wild type and a W335 to leucine variant were isolated with differing quantities of 6-hydroxy-FMN already present in the active site, thereby not necessarily requiring turnover with the substrate.[87,88] A different mechanism involving a flavin iminoquinone methide intermediate mechanism was proposed for the W335L variant of TMADH.[88] The flavin cofactor in TMADH does possess an intrinsic susceptibility to 6-hydroxylation or covalent attachment through a cysteinyl bond; it is interesting to note that varying levels of 6-hydroxylation are present depending on minor changes in the active site environment.[88] Flavins are versatile cofactors, but their potential for catalytic versatility is primarily dictated by the dynamic interactions with the substrate and the protein matrix.[89]

Engineering an enzyme by mutagenesis for new applications has necessarily focused on structure−function relationships, often neglecting protein dynamics, which can have an essential role in enzyme catalysis.[11,22,24,90] Studies that include cofactor dynamics, as in the case of tetracycline resistance enzymes, also showcase that inhibitors can be designed to lock the cofactor flavin in an "inactive" conformation.[82] As our understanding of protein dynamics and the approach for their study further advance, the tools for probing conformational dynamics could be directed toward the rational design of enzymes with novel functions.[7,91,92] The study presented here and the previous computational investigation of *Ec*DHFR demonstrate in different fashions that mutations can modulate the equilibrium between functional and nonfunctional conformational protein ensembles.[11,19] The next challenge is how to apply what is learned about protein dynamics, cofactor motions, and conformational space at the active site to developing new enzyme functions.[91,93] Studies that examine how enzymes have evolved to optimize protein and cofactor motions and organize the active site by conformational transitions will be beneficial for engineering new enzymes that catalyze novel reactions.[14,94−96]

CONCLUSION

In conclusion, our study demonstrates how a simple hydroxyl group can act as a conformational switch. Replacement of a tyrosine with phenylalanine in the active site of *Pa*DADH changed the conformational landscape of the protein, altered the flavin electronic structure, and led to the modification of the cofactor chemical reactivity, ultimately negatively impacting biological function by allowing the formation of an inactive modified flavin in the active site of the enzyme.

ASSOCIATED CONTENT

Accession Codes

*Pa*DADH, UniProtKB Q9HXE3.

AUTHOR INFORMATION

Corresponding Author

Giovanni Gadda − *Department of Chemistry, Department of Biology, and Center for Diagnostics and Therapeutics, Georgia State University, Atlanta, Georgia 30302, United States;* orcid.org/0000-0002-7508-4195; Email: ggadda@gsu.edu

https://dx.doi.org/10.1021/acs.biochem.1c00054
Biochemistry 2021, 60, 711−724

Authors

Archana Iyer − *Department of Chemistry, Georgia State University, Atlanta, Georgia 30302, United States;* orcid.org/0000-0001-5848-4675

Renata A. G. Reis − *Department of Chemistry, Georgia State University, Atlanta, Georgia 30302, United States*

Swathi Gannavaram − *Department of Chemistry, Georgia State University, Atlanta, Georgia 30302, United States*

Mohamed Momin − *Department of Chemistry, Georgia State University, Atlanta, Georgia 30302, United States;* orcid.org/0000-0002-4875-1888

Alexander M. Spring-Connell − *Department of Chemistry, Georgia State University, Atlanta, Georgia 30302, United States*

Yoelvis Orozco-Gonzalez − *Department of Chemistry, Georgia State University, Atlanta, Georgia 30302, United States*

Johnson Agniswamy − *Department of Biology, Georgia State University, Atlanta, Georgia 30302, United States*

Donald Hamelberg − *Department of Chemistry, Georgia State University, Atlanta, Georgia 30302, United States;* orcid.org/0000-0002-3785-3037

Irene T. Weber − *Department of Chemistry and Department of Biology, Georgia State University, Atlanta, Georgia 30302, United States;* orcid.org/0000-0003-4876-7393

Samer Gozem − *Department of Chemistry, Georgia State University, Atlanta, Georgia 30302, United States;* orcid.org/0000-0002-6429-2853

Siming Wang − *Department of Chemistry, Georgia State University, Atlanta, Georgia 30302, United States*

Markus W. Germann − *Department of Chemistry and Department of Biology, Georgia State University, Atlanta, Georgia 30302, United States*

Complete contact information is available at: https://pubs.acs.org/10.1021/acs.biochem.1c00054

Funding

Grant CHE-1506518 from the National Science Foundation partly supported the work. Grant MCB-2018144 from the National Science Foundation partly supported computational studies by M.M. and D.H.

Notes

The authors declare no competing financial interest.

■ ACKNOWLEDGMENTS

The authors thank Dr. Bruce A. Palfey for the generous donation of synthesized 6-OH-FAD. The authors also recognize Daniel Kneller and Shelley Hinkle Burnaman for their valuable input for the X-ray crystallography portion of the project. For assistance during X-ray data collection, the authors thank the staff at the Southeast Regional Collaborative Access Team (SER-CAT) at the Advanced Photon Source (APS), Argonne National Laboratory (ANL). Use of the Advanced Photon Source was supported by the U.S. Department of Energy, Office of Science, Office of Basic Energy Sciences, under Contract W-31-109-Eng-38. Molecular graphics and analyses were performed with UCSF Chimera, developed by the Resource for Biocomputing, Visualization, and Informatics at the University of California, San Francisco, with support from National Institutes of Health Grant P41-GM103311. Y.O.-G. and S. Gozem are grateful to NSF XSEDE for computational resources from research allocation CHE180027 and to the Advanced Research Computing Technology and Innovation Core (ARCTIC) resources supported by NSF-MRI grant CNS-1920024.

■ REFERENCES

(1) Hammes-Schiffer, S. (2013) Catalytic efficiency of enzymes: a theoretical analysis. *Biochemistry 52*, 2012−2020.

(2) Warshel, A., Sharma, P. K., Kato, M., Xiang, Y., Liu, H. B., and Olsson, M. H. M. (2006) Electrostatic basis for enzyme catalysis. *Chem. Rev. 106*, 3210−3235.

(3) Kamerlin, S. C. L., and Warshel, A. (2010) At the dawn of the 21st century: Is dynamics the missing link for understanding enzyme catalysis? *Proteins: Struct., Funct., Genet. 78*, 1339−1375.

(4) Okazaki, K., and Takada, S. (2008) Dynamic energy landscape view of coupled binding and protein conformational change: induced-fit versus population-shift mechanisms. *Proc. Natl. Acad. Sci. U. S. A. 105*, 11182−11187.

(5) Henzler-Wildman, K., and Kern, D. (2007) Dynamic personalities of proteins. *Nature 450*, 964−972.

(6) Kern, D. (2007) Dynamic personality of an enzyme studied by crystallography, NMR, computation and single molecule FRET. *FASEB J. 21*, A90−A90.

(7) Maria-Solano, M. A., Serrano-Hervas, E., Romero-Rivera, A., Iglesias-Fernandez, J., and Osuna, S. (2018) Role of conformational dynamics in the evolution of novel enzyme function. *Chem. Commun. (Cambridge, U. K.) 54*, 6622−6634.

(8) Hammes-Schiffer, S., and Benkovic, S. J. (2006) Relating protein motion to catalysis. *Annu. Rev. Biochem. 75*, 519−541.

(9) van den Bedem, H., and Fraser, J. S. (2015) Integrative, dynamic structural biology at atomic resolution–it's about time. *Nat. Methods 12*, 307−318.

(10) Kraut, D. A., Carroll, K. S., and Herschlag, D. (2003) Challenges in enzyme mechanism and energetics. *Annu. Rev. Biochem. 72*, 517−571.

(11) Bhabha, G., Lee, J., Ekiert, D. C., Gam, J., Wilson, I. A., Dyson, H. J., Benkovic, S. J., and Wright, P. E. (2011) A Dynamic Knockout Reveals That Conformational Fluctuations Influence the Chemical Step of Enzyme Catalysis. *Science 332*, 234−238.

(12) Iorgu, A. I., Baxter, N. J., Cliff, M. J., Levy, C., Waltho, J. P., Hay, S., and Scrutton, N. S. (2018) Nonequivalence of Second Sphere "Noncatalytic" Residues in Pentaerythritol Tetranitrate Reductase in Relation to Local Dynamics Linked to H-Transfer in Reactions with NADH and NADPH Coenzymes. *ACS Catal. 8*, 11589−11599.

(13) Eisenmesser, E. Z., Bosco, D. A., Akke, M., and Kern, D. (2002) Enzyme dynamics during catalysis. *Science 295*, 1520−1523.

(14) Eisenmesser, E. Z., Millet, O., Labeikovsky, W., Korzhnev, D. M., Wolf-Watz, M., Bosco, D. A., Skalicky, J. J., Kay, L. E., and Kern, D. (2005) Intrinsic dynamics of an enzyme underlies catalysis. *Nature 438*, 117−121.

(15) Ramanathan, A., Savol, A. J., Langmead, C. J., Agarwal, P. K., and Chennubhotla, C. S. (2011) Discovering Conformational Sub-States Relevant to Protein Function. *PLoS One 6*, No. e15827.

(16) Fraser, J. S., and Jackson, C. J. (2011) Mining electron density for functionally relevant protein polysterism in crystal structures. *Cell. Mol. Life Sci. 68*, 1829−1841.

(17) Frauenfelder, H., Sligar, S. G., and Wolynes, P. G. (1991) The energy landscapes and motions of proteins. *Science 254*, 1598−1603.

(18) Baldwin, A. J., Hansen, D. F., Vallurupalli, P., and Kay, L. E. (2009) Measurement of methyl axis orientations in invisible, excited states of proteins by relaxation dispersion NMR spectroscopy. *J. Am. Chem. Soc. 131*, 11939−11948.

(19) Boehr, D. D., McElheny, D., Dyson, H. J., and Wright, P. E. (2006) The dynamic energy landscape of dihydrofolate reductase catalysis. *Science 313*, 1638−1642.

(20) Hartmann, H., Parak, F., Steigemann, W., Petsko, G. A., Ponzi, D. R., and Frauenfelder, H. (1982) Conformational substates in a protein: structure and dynamics of metmyoglobin at 80 K. *Proc. Natl. Acad. Sci. U. S. A. 79*, 4967−4971.

(21) Klinman, J. P., and Kohen, A. (2014) Evolutionary aspects of enzyme dynamics. *J. Biol. Chem. 289*, 30205−30212.
(22) Agarwal, P. K. (2006) Enzymes: An integrated view of structure, dynamics and function. *Microb. Cell Fact. 5*, 2.
(23) Fraser, J. S., Clarkson, M. W., Degnan, S. C., Erion, R., Kern, D., and Alber, T. (2009) Hidden alternative structures of proline isomerase essential for catalysis. *Nature 462*, 669−U149.
(24) Jackson, C. J., Foo, J. L., Tokuriki, N., Afriat, L., Carr, P. D., Kim, H. K., Schenk, G., Tawfik, D. S., and Ollis, D. L. (2009) Conformational sampling, catalysis, and evolution of the bacterial phosphotriesterase. *Proc. Natl. Acad. Sci. U. S. A. 106*, 21631−21636.
(25) Camilloni, C., Sahakyan, A. B., Holliday, M. J., Isern, N. G., Zhang, F., Eisenmesser, E. Z., and Vendruscolo, M. (2014) Cyclophilin A catalyzes proline isomerization by an electrostatic handle mechanism. *Proc. Natl. Acad. Sci. U. S. A. 111*, 10203−10208.
(26) Yuan, H., Fu, G., Brooks, P. T., Weber, I., and Gadda, G. (2010) Steady-state kinetic mechanism and reductive half-reaction of D-arginine dehydrogenase from Pseudomonas aeruginosa. *Biochemistry 49*, 9542−9550.
(27) Li, C., and Lu, C. D. (2009) Arginine racemization by coupled catabolic and anabolic dehydrogenases. *Proc. Natl. Acad. Sci. U. S. A. 106*, 906−911.
(28) Gannavaram, S., Sirin, S., Sherman, W., and Gadda, G. (2014) Mechanistic and computational studies of the reductive half-reaction of tyrosine to phenylalanine active site variants of D-arginine dehydrogenase. *Biochemistry 53*, 6574−6583.
(29) Fitzpatrick, P. F. (2010) Oxidation of amines by flavoproteins. *Arch. Biochem. Biophys. 493*, 13−25.
(30) Bradford, M. M. (1976) A rapid and sensitive method for the quantitation of microgram quantities of protein utilizing the principle of protein-dye binding. *Anal. Biochem. 72*, 248−254.
(31) Noble, J. E. (2014) Quantification of protein concentration using UV absorbance and Coomassie dyes. *Methods Enzymol. 536*, 17−26.
(32) Mayhew, S. G., Whitfield, C. D., Ghisla, S., and Schuman-Jorns, M. (1974) Identification and properties of new flavins in electron-transferring flavoprotein from Peptostreptococcus elsdenii and pig-liver glycolate oxidase. *Eur. J. Biochem. 44*, 579−591.
(33) Liu, M. L., Mao, X. A., Ye, C. H., Huang, H., Nicholson, J. K., and Lindon, J. C. (1998) Improved WATERGATE pulse sequences for solvent suppression in NMR spectroscopy. *J. Magn. Reson. 132*, 125−129.
(34) Battye, T. G., Kontogiannis, L., Johnson, O., Powell, H. R., and Leslie, A. G. (2011) iMOSFLM: a new graphical interface for diffraction-image processing with MOSFLM. *Acta Crystallogr., Sect. D: Biol. Crystallogr. 67*, 271−281.
(35) Evans, P. (2006) Scaling and assessment of data quality. *Acta Crystallogr., Sect. D: Biol. Crystallogr. 62*, 72−82.
(36) Fu, G., Yuan, H., Li, C., Lu, C. D., Gadda, G., and Weber, I. T. (2010) Conformational changes and substrate recognition in Pseudomonas aeruginosa D-arginine dehydrogenase. *Biochemistry 49*, 8535−8545.
(37) McCoy, A. J., Grosse-Kunstleve, R. W., Adams, P. D., Winn, M. D., Storoni, L. C., and Read, R. J. (2007) Phaser crystallographic software. *J. Appl. Crystallogr. 40*, 658−674.
(38) Afonine, P. V., Grosse-Kunstleve, R. W., Echols, N., Headd, J. J., Moriarty, N. W., Mustyakimov, M., Terwilliger, T. C., Urzhumtsev, A., Zwart, P. H., and Adams, P. D. (2012) Towards automated crystallographic structure refinement with phenix.refine. *Acta Crystallogr., Sect. D: Biol. Crystallogr. 68*, 352−367.
(39) Emsley, P., Lohkamp, B., Scott, W. G., and Cowtan, K. (2010) Features and development of Coot. *Acta Crystallogr., Sect. D: Biol. Crystallogr. 66*, 486−501.
(40) Moriarty, N. W., Grosse-Kunstleve, R. W., and Adams, P. D. (2009) electronic Ligand Builder and Optimization Workbench (eLBOW): a tool for ligand coordinate and restraint generation. *Acta Crystallogr., Sect. D: Biol. Crystallogr. 65*, 1074−1080.
(41) Pettersen, E. F., Goddard, T. D., Huang, C. C., Couch, G. S., Greenblatt, D. M., Meng, E. C., and Ferrin, T. E. (2004) UCSF Chimera–a visualization system for exploratory research and analysis. *J. Comput. Chem. 25*, 1605−1612.
(42) Maier, J. A., Martinez, C., Kasavajhala, K., Wickstrom, L., Hauser, K. E., and Simmerling, C. (2015) ff14SB: Improving the Accuracy of Protein Side Chain and Backbone Parameters from ff99SB. *J. Chem. Theory Comput. 11*, 3696−3713.
(43) Cornell, W. D., Cieplak, P., Bayly, C. I., Gould, I. R., Merz, K. M., Ferguson, D. M., Spellmeyer, D. C., Fox, T., Caldwell, J. W., and Kollman, P. A. (1995) A Second Generation Force Field for the Simulation of Proteins, Nucleic Acids, and Organic Molecules. *J. Am. Chem. Soc. 117*, 5179−5197.
(44) Wang, J., Wolf, R. M., Caldwell, J. W., Kollman, P. A., and Case, D. A. (2004) Development and testing of a general amber force field. *J. Comput. Chem. 25*, 1157−1174.
(45) Mark, P., and Nilsson, L. (2001) Structure and Dynamics of the TIP3P, SPC, and SPC/E Water Models at 298 K. *J. Phys. Chem. A 105*, 9954−9960.
(46) Jorgensen, W. (1982) Revised TIPS for simulations of liquid water and aqueous solutions. *J. Chem. Phys. 77*, 4156−4163.
(47) Momin, M., Yao, X. Q., Thor, W., and Hamelberg, D. (2018) Substrate Sequence Determines Catalytic Activities, Domain-Binding Preferences, and Allosteric Mechanisms in Pin1. *J. Phys. Chem. B 122*, 6521−6527.
(48) Darden, T., York, D., and Pedersen, L. (1993) Particle mesh Ewald: An N·log(N) method for Ewald sums in large systems. *J. Chem. Phys. 98*, 10089−10092.
(49) Ryckaert, J.-P., Ciccotti, G., and Berendsen, H. J. C. (1977) Numerical integration of the cartesian equations of motion of a system with constraints: molecular dynamics of n-alkanes. *J. Comput. Phys. 23*, 327−341.
(50) Roe, D. R., and Cheatham, T. E., 3rd. (2013) PTRAJ and CPPTRAJ: Software for Processing and Analysis of Molecular Dynamics Trajectory Data. *J. Chem. Theory Comput. 9*, 3084−3095.
(51) Orozco-Gonzalez, Y., Manathunga, M., Marin, M. D. C., Agathangelou, D., Jung, K. H., Melaccio, F., Ferre, N., Haacke, S., Coutinho, K., Canuto, S., and Olivucci, M. (2017) An Average Solvent Electrostatic Configuration Protocol for QM/MM Free Energy Optimization: Implementation and Application to Rhodopsin Systems. *J. Chem. Theory Comput. 13*, 6391−6404.
(52) Singh, U. C., and Kollman, P. A. (1986) A combined ab initio quantum mechanical and molecular mechanical method for carrying out simulations on complex molecular systems: Applications to the CH3Cl + Cl- exchange reaction and gas phase protonation of polyethers. *J. Comput. Chem. 7*, 718−730.
(53) Humbel, S., Sieber, S., and Morokuma, K. (1996) The IMOMO method: Integration of different levels of molecular orbital approximations for geometry optimization of large systems: Test for n-butane conformation and SN2 reaction: RCl+Cl-. *J. Chem. Phys. 105*, 1959−1967.
(54) Hornak, V., Abel, R., Okur, A., Strockbine, B., Roitberg, A., and Simmerling, C. (2006) Comparison of multiple Amber force fields and development of improved protein backbone parameters. *Proteins: Struct., Funct., Genet. 65*, 712−725.
(55) Hornak, V., Okur, A., Rizzo, R. C., and Simmerling, C. (2006) HIV-1 protease flaps spontaneously open and reclose in molecular dynamics simulations. *Proc. Natl. Acad. Sci. U. S. A. 103*, 915−920.
(56) Jorgensen, W. L., Chandrasekhar, J., Madura, J. D., Impey, R. W., and Klein, M. L. (1983) Comparison of simple potential functions for simulating liquid water. *J. Chem. Phys. 79*, 926−935.
(57) Pronk, S., Pall, S., Schulz, R., Larsson, P., Bjelkmar, P., Apostolov, R., Shirts, M. R., Smith, J. C., Kasson, P. M., van der Spoel, D., Hess, B., and Lindahl, E. (2013) GROMACS 4.5: a high-throughput and highly parallel open source molecular simulation toolkit. *Bioinformatics 29*, 845−854.
(58) Coutinho, K., Georg, H. C., Fonseca, T. L., Ludwig, V., and Canuto, S. (2007) An efficient statistically converged average configuration for solvent effects. *Chem. Phys. Lett. 437*, 148−152.
(59) Aquilante, F., De Vico, L., Ferre, N., Ghigo, G., Malmqvist, P. A., Neogrady, P., Pedersen, T. B., Pitonak, M., Reiher, M., Roos, B. O.,

https://dx.doi.org/10.1021/acs.biochem.1c00054
Biochemistry 2021, 60, 711−724

Serrano-Andres, L., Urban, M., Veryazov, V., and Lindh, R. (2010) MOLCAS 7: the next generation. *J. Comput. Chem. 31*, 224−247.
(60) Ponder, J. W., and Case, D. A. (2003) Force fields for protein simulations. *Adv. Protein Chem. 66*, 27−85.
(61) Strambi, A., Coto, P. B., Frutos, L. M., Ferré, N., and Olivucci, M. (2008) Relationship between the Excited State Relaxation Paths of Rhodopsin and Isorhodopsin. *J. Am. Chem. Soc. 130*, 3382−3388.
(62) Roos, B. O. (2007) The Complete Active Space Self-Consistent Field Method and its Applications in Electronic Structure Calculations. *In Adv. Chem. Phys.*, 399−445.
(63) Widmark, P.-O., Malmqvist, P.-Å., and Roos, B. O. (1990) Density matrix averaged atomic natural orbital (ANO) basis sets for correlated molecular wave functions. *Theor. Chem. Acc. 77*, 291−306.
(64) Bayly, C. I., Cieplak, P., Cornell, W. D., and Kollman, P. A. (1993) A Well-Behaved Electrostatic Potential Based Method Using Charge Restraints for Deriving Atomic Charges - the Resp Model. *J. Phys. Chem. 97*, 10269−10280.
(65) Lee, C., Yang, W., and Parr, R. G. (1988) Development of the Colle-Salvetti correlation-energy formula into a functional of the electron density. *Phys. Rev. B: Condens. Matter Mater. Phys. 37*, 785−789.
(66) Kabir, M. P., Orozco-Gonzalez, Y., and Gozem, S. (2019) Electronic spectra of flavin in different redox and protonation states: a computational perspective on the effect of the electrostatic environment. *Phys. Chem. Chem. Phys. 21*, 16526−16537.
(67) Choe, Y.-K., Nagase, S., and Nishimoto, K. (2007) Theoretical study of the electronic spectra of oxidized and reduced states of lumiflavin and its derivative. *J. Comput. Chem. 28*, 727−739.
(68) Gozem, S., Luk, H. L., Schapiro, I., and Olivucci, M. (2017) Theory and Simulation of the Ultrafast Double-Bond Isomerization of Biological Chromophores. *Chem. Rev. 117*, 13502−13565.
(69) Schollnhammer, G., and Hemmerich, P. (1974) Nucleophilic addition at the photoexcited flavin cation: synthesis and properties of 6- and 9-hydroxy-flavocoenzyme chromophores. *Eur. J. Biochem. 44*, 561−577.
(70) Huang, C. H., Winkler, A., Chen, C. L., Lai, W. L., Tsai, Y. C., Macheroux, P., and Liaw, S. H. (2008) Functional roles of the 6-S-cysteinyl, 8alpha-N1-histidyl FAD in glucooligosaccharide oxidase from Acremonium strictum. *J. Biol. Chem. 283*, 30990−30996.
(71) Huang, L., Scrutton, N. S., and Hille, R. (1996) Reaction of the C30A mutant of trimethylamine dehydrogenase with diethylmethylamine. *J. Biol. Chem. 271*, 13401−13406.
(72) Ghisla, S., Kenney, W. C., Knappe, W. R., McIntire, W., and Singer, T. P. (1980) Chemical synthesis and some properties of 6-substituted flavins. *Biochemistry 19*, 2537−2544.
(73) Ghisla, S., Massey, V., and Yagi, K. (1986) Preparation and some properties of 6-substituted flavins as active site probes for flavin enzymes. *Biochemistry 25*, 3282−3289.
(74) Ghisla, S., and Mayhew, S. G. (1976) Identification and properties of 8-hydroxyflavin–adenine dinucleotide in electron-transferring flavoprotein from Peptostreptococcus elsdenii. *Eur. J. Biochem. 63*, 373−390.
(75) Massey, V., Ghisla, S., and Yagi, K. (1986) 6-Azido- and 6-aminoflavins as active-site probes of flavin enzymes. *Biochemistry 25*, 8095−8102.
(76) Lu, X., Nikolic, D., Mitchell, D. J., van Breemen, R. B., Mersfelder, J. A., Hille, R., and Silverman, R. B. (2003) A mechanism for substrate-Induced formation of 6-hydroxyflavin mononucleotide catalyzed by C30A trimethylamine dehydrogenase. *Bioorg. Med. Chem. Lett. 13*, 4129−4132.
(77) Gatti, D. L., Palfey, B. A., Lah, M. S., Entsch, B., Massey, V., Ballou, D. P., and Ludwig, M. L. (1994) The mobile flavin of 4-OH benzoate hydroxylase. *Science 266*, 110−114.
(78) David, C. C., and Jacobs, D. J. (2014) Principal component analysis: a method for determining the essential dynamics of proteins. *Methods Mol. Biol. 1084*, 193−226.
(79) Agarwal, P. K. (2005) Role of protein dynamics in reaction rate enhancement by enzymes. *J. Am. Chem. Soc. 127*, 15248−15256.
(80) Crozier-Reabe, K., and Moran, G. R. (2012) Form follows function: structural and catalytic variation in the class a flavoprotein monooxygenases. *Int. J. Mol. Sci. 13*, 15601−15639.
(81) Zheng, Y., Dong, J., Palfey, B. A., and Carey, P. R. (1999) Using Raman spectroscopy to monitor the solvent-exposed and "buried" forms of flavin in p-hydroxybenzoate hydroxylase. *Biochemistry 38*, 16727−16732.
(82) Park, J., Gasparrini, A. J., Reck, M. R., Symister, C. T., Elliott, J. L., Vogel, J. P., Wencewicz, T. A., Dantas, G., and Tolia, N. H. (2017) Plasticity, dynamics, and inhibition of emerging tetracycline resistance enzymes. *Nat. Chem. Biol. 13*, 730−736.
(83) Setser, J. W., Heemstra, J. R., Jr., Walsh, C. T., and Drennan, C. L. (2014) Crystallographic evidence of drastic conformational changes in the active site of a flavin-dependent N-hydroxylase. *Biochemistry 53*, 6063−6077.
(84) Manenda, M. S., Picard, M. E., Zhang, L., Cyr, N., Zhu, X., Barma, J., Pascal, J. M., Couture, M., Zhang, C., and Shi, R. (2020) Structural analyses of the Group A flavin-dependent monooxygenase PieE reveal a sliding FAD cofactor conformation bridging OUT and IN conformations. *J. Biol. Chem. 295*, 4709−4722.
(85) Campbell, A. C., Stiers, K. M., Martin Del Campo, J. S., Mehra-Chaudhary, R., Sobrado, P., and Tanner, J. J. (2020) Trapping conformational states of a flavin-dependent N-monooxygenase in crystallo reveals protein and flavin dynamics. *J. Biol. Chem. 295*, 13239−13249.
(86) Miura, R. (2001) Versatility and specificity in flavoenzymes: control mechanisms of flavin reactivity. *Chem. Rec. 1*, 183−194.
(87) Trickey, P., Basran, J., Lian, L. Y., Chen, Z., Barton, J. D., Sutcliffe, M. J., Scrutton, N. S., and Mathews, F. S. (2000) Structural and biochemical characterization of recombinant wild type and a C30A mutant of trimethylamine dehydrogenase from methylophilus methylotrophus (sp. W(3)A(1)). *Biochemistry 39*, 7678−7688.
(88) Mewies, M., Basran, J., Packman, L. C., Hille, R., and Scrutton, N. S. (1997) Involvement of a flavin iminoquinone methide in the formation of 6-hydroxyflavin mononucleotide in trimethylamine dehydrogenase: a rationale for the existence of 8alpha-methyl and C6-linked covalent flavoproteins. *Biochemistry 36*, 7162−7168.
(89) Piano, V., Palfey, B. A., and Mattevi, A. (2017) Flavins as Covalent Catalysts: New Mechanisms Emerge. *Trends Biochem. Sci. 42*, 457−469.
(90) Furst, M., Romero, E., Gomez Castellanos, J. R., Fraaije, M. W., and Mattevi, A. (2018) Side-Chain Pruning Has Limited Impact on Substrate Preference in a Promiscuous Enzyme. *ACS Catal. 8*, 11648−11656.
(91) Bhabha, G., Biel, J. T., and Fraser, J. S. (2015) Keep on moving: discovering and perturbing the conformational dynamics of enzymes. *Acc. Chem. Res. 48*, 423−430.
(92) Gardner, J. M., Biler, M., Risso, V. A., Sanchez-Ruiz, J. M., and Kamerlin, S. C. L. (2020) Manipulating Conformational Dynamics To Repurpose Ancient Proteins for Modern Catalytic Functions. *ACS Catal. 10*, 4863−4870.
(93) Tokuriki, N., and Tawfik, D. S. (2009) Protein dynamism and evolvability. *Science 324*, 203−207.
(94) Pandya, C., Farelli, J. D., Dunaway-Mariano, D., and Allen, K. N. (2014) Enzyme promiscuity: engine of evolutionary innovation. *J. Biol. Chem. 289*, 30229−30236.
(95) Pabis, A., Risso, V. A., Sanchez-Ruiz, J. M., and Kamerlin, S. C. (2018) Cooperativity and flexibility in enzyme evolution. *Curr. Opin. Struct. Biol. 48*, 83−92.
(96) Crean, R. M., Gardner, J. M., and Kamerlin, S. C. L. (2020) Harnessing Conformational Plasticity to Generate Designer Enzymes. *J. Am. Chem. Soc. 142*, 11324−11342.

https://dx.doi.org/10.1021/acs.biochem.1c00054
Biochemistry 2021, 60, 711−724